Blood Glucose Monitoring and Communicative Implantable Chip Using a Wireless Power Transfer

Hyeonkeon Lee[$1], Honghyeon Park[*2] and Sanghoek Kim[^3]
[$]LIG Nex1 Co., Ltd, South Korea
[*]Silicon Mitus Inc, South Korea
[^]Department of Electronics and Information Engineering, Kyung Hee University, South Korea
E-mail : [1]hkeon2@khu.ac.kr, [2]honghyeon47@gmail.com, [3]sanghoek@khu.ac.kr

***Abstract* - This work proposes a wireless operating system for continuous monitoring of glucose level. The system consists of an implantable device and an external readout transmitter. The implantable device measures a glucose level and wirelessly communicates with the external reader, employing the backscattered modulation for low-power operation. The implantable device converts the light intensity scattered from a fluorescent hydrogel sensor reacting on glucose level to the frequency-modulated signal, and sends this back to the external reader while it is being powered wirelessly. The entire implantable device including the 1000×600-μm^2 die fabricated in TSMC 180-nm CMOS process is bonded on PCB and the fluorescence hydrogel sensor fits in 2×2.5 mm2, and consumes 146.5 μW of power in average during the operation.**

***Keywords*—implantable glucose sensor, backscatter, fluorescent, WPT**

I. INTRODUCTION

Blood glucose monitoring is essential not only for diabetic patients but also for those who do high-intensity exercise or labor, because even healthy people can suffer accidents due to hypoglycemia. However, blood glucose measurement through blood sampling, which is a traditional blood glucose measurement method, requires extra test tools and induces the pain of finger pricking. In addition, since it is difficult to measure blood glucose concentration in real time, response in an emergency would be retardant. Much research has been done to continuous glucose monitoring (CGM) that provides dynamic, continuous blood-glucose information and gives a user an alarm when abnormal blood glucose occurs. Some of them, using wearable devices such as lens-type [1, 2] and bandage-type [3] were proposed for non-invasive CGM, and implantable sensors using glucose oxidase reactions [4, 5] and glucose-sensitive permittivity change [6] were proposed for invasive CGM. Although they present promising results, the previous methods are not sufficient for CGM. Sweat/tear glucose sensors suffer low accuracy and the permittivity of a tissue occurs insufficient selectivity with blood glucose [1, 2, 7, 8].

In contrast, this work proposes to use a fluorescent hydrogel sensor made of di-boronic acid with glucose, which is demonstrating its long-term, accurate continuous glucose monitoring [9]. The chemical forms a bonding with glucose when excited with photons with a specific wavelength and emits photons with an altered wavelength when bonding is broken. The resultant fluorescent level depends on the concentration of the glucose. Therefore, the fluorescent level from the sensor can inform the glucose level. The opacity of skin for a light, however, significantly attenuates the fluorescence intensity after the penetration, making the system susceptible to the ambient light noise. To encircle the problem, implantable sensors that also include the electronic components such as the light emitter and the light detector were proposed [8, 10]. As the result of system integration, however, those systems used to be too bulky to implant. For example, while a recent research presented a fully-implantable, wireless glucose sensor [10], the system necessitates several power-hungry components such as an ADC and a nonvolatile memory, ending up with the entire device size as large as 18.3 mm in length.

From the in-vitro experiment, we demonstrate that the frequency of backscattered signal increases with the glucose level in a dish containing the sensor. Submodules such as the amplifier, the oscillator, and the digital modulator are confirmed to function correctly as designed in experiment. The measurement results are presented in Section IV. The only block that failed to work was the rectifier, which prevented the full operation of the entire implantable system. Specifically, the output voltage of the rectifier was not high enough to turn on the system. The reason for the failure of the rectifier is still under investigation, and the chip should be modified to resolve the issue in the design of next round.

II. SYSTEM DESCRIPTION

A. System Overview

a. Corresponding author; hkeon2@khu.ac.kr

Manuscript Received Apr. 3, 2023, Revised Jun. 17, 2023, Accepted Jun. 18, 2023

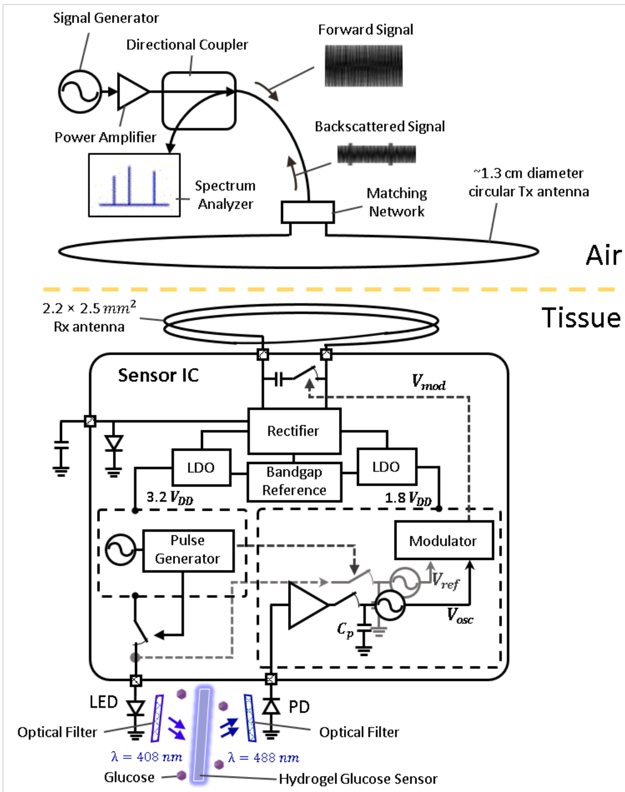

Fig 1. System Overview

The system we present is to be implanted at a depth of about 20 mm under the skin. In this reason, the system should get rid of a battery and be miniaturized. WPT is employed to circumvent using a battery. Since the only WPT is a source to operate the system, most of wireless communication methods are not suitable for an implantable system. Load-Shift Keying (LSK) can have an advantage for a wireless communication method in this regard. Fig 1. shows a diagram of system overview. Tx antenna transmits RF power and receives a backscattered signal. The backscattered signal is shown that amplitude is modulated by LSK. In turn, the backscattered signal is coupled to a spectrum analyzer and the amplitude frequency is revealed on both sides of a carrier frequency. Glucose concentration is higher, the amplitude frequency is further from a carrier frequency. Therefore, the glucose concentration can be read out of skin. Since the sensor IC only needs to shift the Rx antenna impedance, it does not consume extra energy for communication.

Sensor IC changes the RF power to DC power to operate LED, amplifiers, oscillators, a pulse generator and a modulator. Rectifier and Low-Drop Out regulator (LDO) are utilized in this conversion. An external capacitor and a limiter diode is connected to the output of rectifier, so the external capacitor stores converted DC power and the limiter diode protects the other circuits from overvoltage. Two LDOs adhere to the rectifier, one for LED generates 3.2 V_{DD} and the other 1.8 V_{DD} for the sensing part.

An oscillator and a pulse generator control the switch that turns a LED on and off and the switches in the sensing part. By turning on and off the LED, power consumption and photo bleaching of a hydrogel sensor can be diminished. Since the switching for LED causes overshoot when it turns on and off, the pulse for sensing part has shorter duty than the LED. The glucose information stored in the capacitor C_p change the frequency V_{OSC} of VCO, and it is modulated with V_{ref} which is of LED luminance intensity. V_{mod}, the pulsed output of modulator shifts the impedance of antenna whose pulse frequency is informed by the glucose concentration, and pulse width is informed by the LED luminance intensity.

B. *Fluorescent Hydrogel Glucose Sensor*

Although this paper is focused on the electronics, an overview of the fluorescent sensor provided in this section is included to explain the complete system. The di-boronic acid used as a glucose detector has a long life span suitable for use as Continuous Glucose Monitoring (CGM) because it can react reversibly to glucose without other reagents or enzymes. Also, it is appropriate as an implantable glucose sensor because the sensor is polymerized with a highly biocompatible polyacrylamide hydrogel [5]. When the LED excites an ultra-violet (UV) light, the sensor absorbs it and emits UV light with a longer wavelength as a response. The emission light intensity of the sensor is varied by glucose concentrations. Therefore, the fluorescence intensity corresponds to the glucose concentrations. For the measurement of the fluorescence intensity, the photodiode is employed as a photodetector. Specifically, the wavelength of the LED excitation light is around 408nm while the wavelength of the shifted emission light is around 488nm. Therefore, optical bandpass filters are attached in front of the LED and the photodiode to block the direct coupling from the LED to the photodiode bypassing the hydrogel glucose sensor.

C. *Architectural Overview of the Sensor Electronics*

In order to measure biological signals in the body and read them in-vitro, an electronic system is required to convert the biological signals into electrical signals and communicate with the external system. Simultaneously, the sensor electronic receives the power to operate the system. In this section, the architecture of sensor electronics in the right box of the Fig. 1 is explained.

The rectifier changing the RF power into DC is the fundamental component for RF energy harvesting. In addition, the regulator must stabilize the harvested DC voltage from rectifier. To provide an accurate DC voltage regardless of environment, a bandgap reference is employed in the regulator. Since we utilize an off-chip LED which necessitate a high voltage, there are two regulators, one for the LED operation (3.3 V) and the other for a core system (1.8 V). Since the high voltage along with the high current through the LED consumes high power, we limit a turn-on duration of the LED by using a pulse generator.

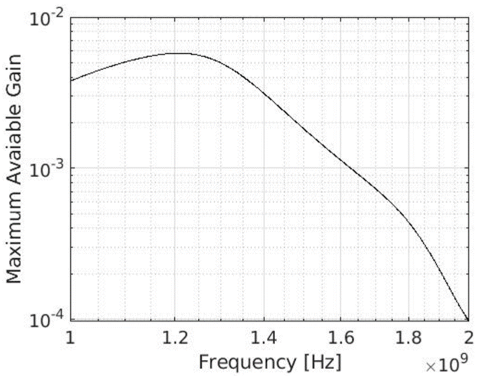

Fig. 2. Maximum available gain

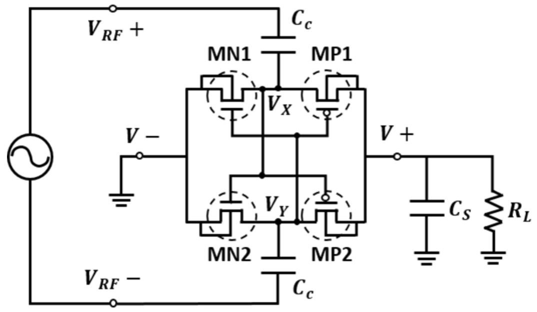

Fig. 3. Single stage cross-coupled rectifier

This is also beneficial to lengthen the lifetime of hydrogel glucose sensor by reducing the exposure time of sensor to light, which may lead to photo-bleaching of the sensor. The pulse excitation of the LED, however, would also make the excited current through the photodiode pulse-shaped. In order for VCO to oscillate in a constant frequency corresponding to the glucose level, the input voltage of the VCO must be static and sampled while the LED is on. For this end, a switch controlled by the pulse generator is used to sample and hold the charge pumped by the photodiode across the capacitor at the input of the VCO. The oscillating voltage of the VCO is converted to the pulse train through the digital modulating block, and the pulse switches the transistor to shift the load impedance.

III. CIRCUIT IMPLEMENTATION

A. Power Delivery and Management

Before designing the power components, the operation frequency of wireless powering should be decided to optimize the power transfer efficiency. The electromagnetic simulation is conducted by a commercial simulator Ansys HFSS to decide the frequency for a given receive and transmit antenna structure.

At first, the configuration of the receiver is designed based on the predicted size of PCB on which the chip and the discrete components such as the storage capacitor, the LED, and the photodiode are mounted. This accordingly decides the size of the receiver loop antenna. Since the loop antenna is small compared to the wavelength of typical frequency for WPT, it may be modeled as a magnetic dipole receiver.

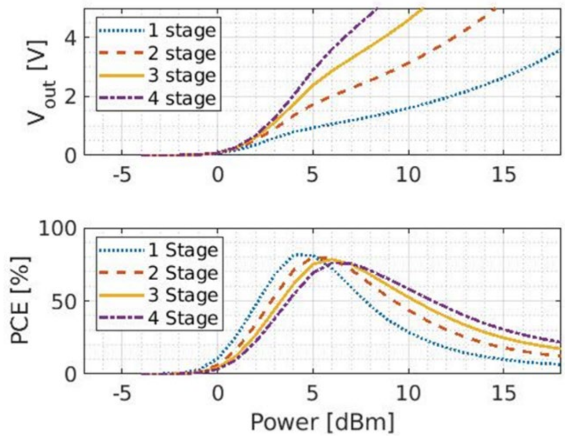

Fig. 4. Power conversion efficiency

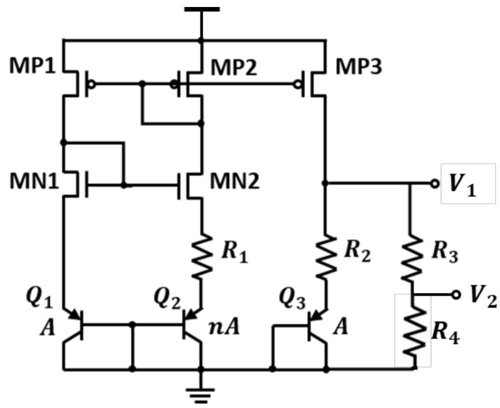

Fig. 5. Bandgap reference

Secondly, the transmitter is configured by the optimal current source to power the magnetic dipole receiver [11]-[12]. Fig. 2 shows a maximum available gain (MAG) which is deduced from the s-parameters of the electromagnetic simulation:

$$MAG = \frac{|S_{21}|}{|S_{12}|}\left(K - \sqrt{K^2 - 1}\right) \tag{1}$$

$$K = \frac{1 - |S_{11}|^2 - |S_{22}|^2 + |\Delta|^2}{2 \cdot |S_{21}S_{12}|} \tag{2}$$

, where $\Delta = S_{11}S_{22} - S_{12}S_{21}$, and the MAG can be obtained with impedance fully matched. From the peak of Fig. 2, we decide 1.2 GHz as the operation frequency.

Traditional rectifier has a threshold voltage in the diode, and it debases the power conversion efficiency of rectifier. Cross-coupled invertor structure in the Fig. 3 is useful for self-threshold voltage cancelation, and it also reduces leakage current for inversed bias [13]. Fig. 4 shows simulation results of a power conversion efficiency versus the input power according to the number of stages at 1.2 GHz. Three stage has the highest efficiency for the target unregulated voltage of 3.3 V and the load of 180 kΩ. Since the efficiency decreases after the target voltage, it operates as a kind of limiter as well. For the impedance conjugate matching, the input impedance when the rectifier output voltage reached at 3.3 V is matched to the receiver antenna with a capacitor on the IC.

A bandgap reference is the most commonly used circuit to obtain the voltage and temperature independent reference [14]. Self-biasing structure accomplishes the voltage

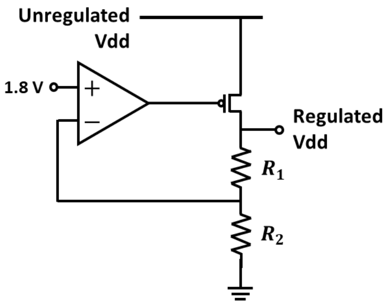

Fig. 6. Low drop-out regulator

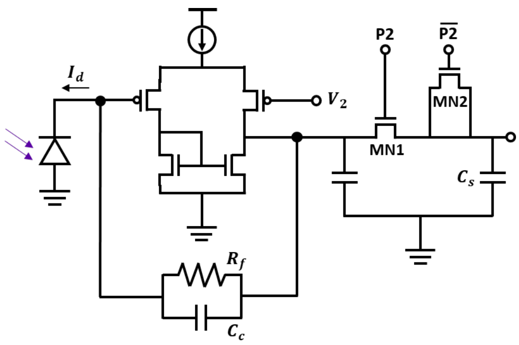

Fig. 7. Trans-impedance amplifier

independence, and the combination of PTAT and CTAT attains temperature independence as shown in Fig. 5. Such a reference is used to bias regulator and sensor signal amplifier, and also the current is mirrored to biasing amplifiers. Reference voltage V_1 is for the regulator, and V_2 is for the sensing amplifier. However, if the unregulated voltage is too high when the incoming RF power exceeds a certain threshold, bandgap reference can be damaged. Therefore, additional diodes are employed as a voltage limiter to lower the voltage when it exceeds some point (not shown).

This system requires two regulators to supply two levels voltage for LED and readout modules. Low drop-out (LDO) circuit is adopted as a regulator. The chosen LDO circuits are shown in the Fig. 6. The first LDO is used to provide 3-V Vdd to LED. The ratio of R_1 to R_2 is 0.561. The second LDO is used to provide 1.8-V Vdd to the readout modules. It is almost identical structure with a former, but since the target Vdd value is the same as the output voltage of the bandgap reference circuit, the resistors (R_1, R_2) for upconverting output voltage are not necessary. Instead, the output node is directly connected to the negative input of the amplifier, while the positive input of op-amp is connected to the bandgap reference circuit.

The gain of amplifier should be large enough so that the regulated voltage is not affected by the unregulated Vdd. The gain of the amplifier is set to be 20 dB. To satisfy the stability, LDO has the bandwidth as ten times wide as the ripple frequency of loads. This leads that the bandwidth of LDOs should be larger than 4 MHz.

B. *Transimpedance amplifier with switching capacitor*

The trans-impedance amplifier (TIA) is typically used to amplify the signal of photodiode [15]. The photodiode signal (current) is converted to voltage by TIA. As shown in Fig. 7, the negative input of TIA is connected to cathode of photodiode while the positive input V_2 takes from the bandgap reference. The current of photodiode I_d is converted to high voltage as it goes through a large resistor R_f. To decide the target gain, in prior to the IC design, the current of photodiode device is measured to be from 80 nA to 100 nA for the expected light intensity. This current needs to be amplified to a few mV scales. So, the closed loop gain is set to be 120 dBΩ. A feedback capacitor C_c is used for stability compensation.

To save the power, the duty cycle of photodiode current is set to be only 1%. So, the charge needs to be stored during the turn-on period to the storage capacitor, C_s, using the switch MN1 before the ring oscillator. The switch MN1 should be controlled in a synchronization with the signal that turns on the LED. Explicitly, the control pulse P2 has 0.5% duty cycle and is delayed by 50 μs compared to LED pulse. Then, when the photodiode is turned on by the scattered light from the fluorescent sensor excited by the LED, the switch passes the charge generated by the photodiode to the storage capacitor. After the duty cycle, the switch is turned off and hold the charge across the storage capacitor.

It is well known that the charge injection [16] occurs when the switching capacitor alters on and off, introducing errors in detecting a small signal. To suppress the error by the charge injection, the dummy switch MN2 is added to load node and operated by the inverse signal of P2. This dummy switch acquires the same amount of channel charge that main switch should lose and calibrates out the error.

The bandwidth of the amplifier is decided based on the pulse width. The period of LED pulse is 10 ms and pulse width is 100 μs (1% duty cycle). For the amplifier reacts fast enough during this pulse width, the target bandwidth of the amplifier is set to be five-times higher than 10 kHz. Satisfying the listed specifications along with the target dynamic range is 60 dB, the amplifier is designed to operate with the minimum power, which results in the power consumption fewer than 4 μW.

C. *Voltage-to-Frequency Converter*

The output voltage of readout amplifier drives the current control transistor MN, whose current is mirrored to a ring oscillator-based voltage-to-frequency (*V-to-F*) converter as shown in Fig. 8. The oscillator normally operates at 10 kHz and consumes average 10 μA. The mirrored current changes the charging and discharging time of inverter and, consequently, controls the output frequency exactly. As the current mirrors control the current, oscillator can be operated as current-starved. The oscillation frequency of current-starved ring oscillator can be expressed as

$$f_{osc} = \frac{I_d}{N \bullet C_{total} \bullet V_{dd}} \quad (3)$$

where I_d is the current of each stage, N is the number of stages, V_{dd} is the supply voltage and C_{total} is capacitance

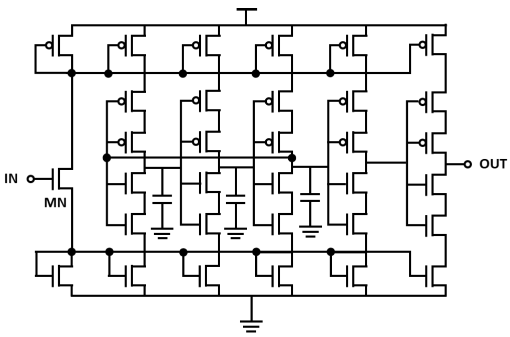

Fig. 8. Current-starved voltage controlled ring oscillator

at the output of each stage. As shown the above relation, output frequency varies linearly following the current. Two inverters are improved as a buffer for prevent interference from the digital part. Buffers are also current-starved structure.

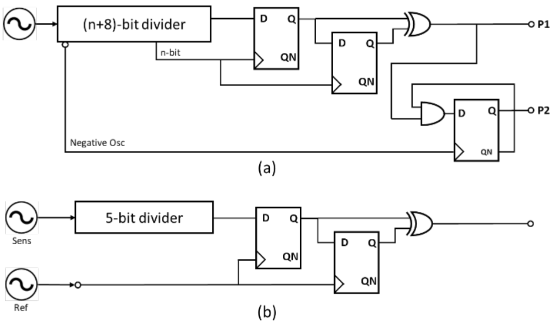

Fig. 9. Pulse generator for (a) LED, and (b) modulator

D. Pulse Generator and Backscatter Modulator

Although the pulse generator and the modulator are used for different purposes, they share the same configuration. A pulse is logically generated by using D flip-flops and XOR [1]. The logic is validated with a Verilog before designing a circuit. Two waves, one of which is much slower than the other, are to be an input of the digital logic. The slow enters D as a signal, and the fast is used as a clock of D flip-flops. The slower wave is related on pulse frequency and the fast is related on the pulse width. Accordingly, a pulse generator for LED has inputs that the slower is about one hundred times slower divided by the frequency divider to adjust 1% duration as shown in Fig. 9(a). The P1 is for turning LED on and off, and the P2 is for the switched capacitor. For protecting against overshooting noise that occurs on the edge of LED pulse, the P2 rises a half cycle after the clock and falls a half cycle early than the clock. On the other hand, the modulator has a different frequency source, because both the sensed data and reference data should be transferred as shown in Fig. 9(b). Sensed data frequency is divided by about ten to adjust 10% duration.

The counter circuit is used not only as a frequency divider but also as a circuit to reduce frequency drift. Since common VCO circuits without PLL suffer from frequency drift as a phase noise, the counter can be applied to average the frequency drift so that reduce the phase noise in time domain.

IV. MEASUREMENT RESULTS

The chip was implemented by TSMC 180-nm CMOS process. Fig. 10 shows a photograph of the readout IC. The chip area is $1 \times 0.6\ mm^2$. For the in-vitro test, the bare chip is wire-bonded to the PCB with coated PDMS and inserted in a phantom tissue would mimic the real human tissue.

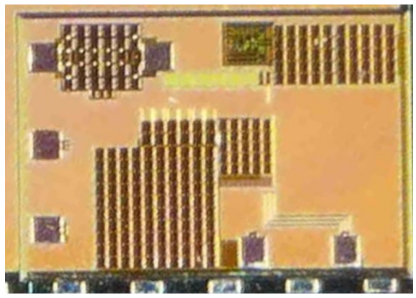

Fig. 10. Photograph of fabricated readout IC

A. Power Management Block

To test the LDO performance, the load modules are replaced by the equivalent resistor and capacitor. The LDO for LED is tested assuming the worst-case scenario where the resistor equivalent to the LED remaining always on is used as the load module. Fig. 11 shows and compares the result of the simulation and the measurement. The measured result follows the simulation result well. The bandwidth of LDO can be measured in the time domain using an oscilloscope. Fig. 12 shows at the moment when the LED turns on, the LDO voltage drops suddenly. Its voltage will be recovered in a fraction of a microsecond by the feedback loop with the amplifier. The bandwidth of amplifier is calculated to be the reciprocal of the recovering time. Using this method, the measured bandwidth is 4.5 MHz, which is close to the designed one in simulation, 4 MHz.

B. Signal Conditioning Block

To check the functionality of the signal conditioning block, including the TIA, VCO, and the modulation block, the external DC power was supplied to the implantable system excluding the rectifier block. The distance between photodiode and LED was 0.8 mm. In real application, the LED should light the fluorescent sensor and the photodiode should be excited by the light emitted by the fluorescent sensor. The optical bandpass filter should be properly placed to block bypassing light from the LED to the photodiode. In this experiment that concentrates to evaluate the functionality of the electronics, the light is allowed to directly transfer from the LED to the photodiode without a fluorescent sensor. The input light intensity for the photodiode was controlled by the number of semi-transparent tapes applied between the LED and the photodiode. The more number of tapes applied, the dimmer light would enter into the photodiode, as mimicking that the fluorescence intensity weakens when the glucose concentration decreases. When the number of applied tapes varies from zero to four, Fig. 13(a) shows how the pulse period changes in time domain. While the pulse width is fixed as 7 μs, and the pulse period increased from 0.1 to 0.25 ms. The measurement of the pulse in the frequency domain is shown in Fig. 13(b) according to the number of tapes applied. The experiment was repeated by

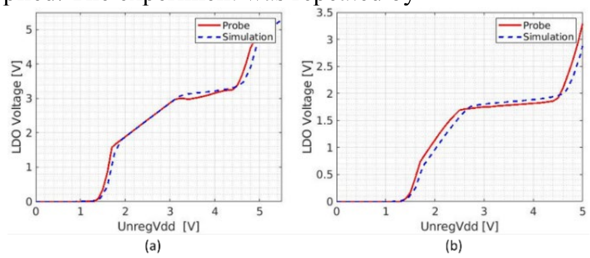

Fig. 11. Measured result of regulator for (a) LED, and (b) core system

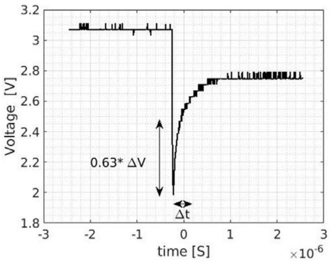

Fig. 12. LDO output voltage measurement in transient domain

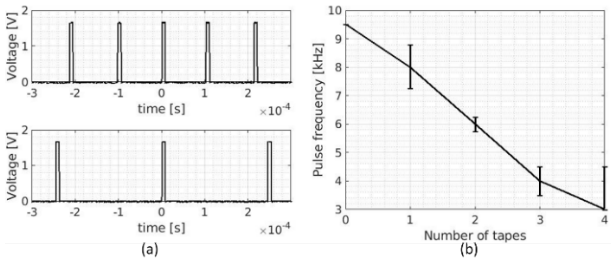

Fig. 13. Measurement result of modulated sensing signal varying the light intensity (a) in time domain, and (b) versus the light intensity

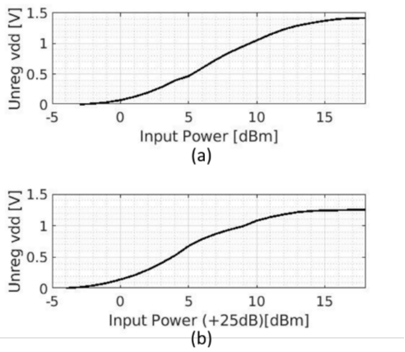

Fig. 14. Power conversion measurement of rectifier

three times and the error bar shows the spread of the measured frequency. It clearly shows that as the number of tapes increases, the light intensity is dimmed, reducing the output frequency of the pulse signal.

C. *Wireless Power Delivery*

For verification of rectifier and wireless power delivery, measurement is conducted by two experiments. First, the rectifier was connected to SMA connector through the PCB without antenna. A function generator sent the RF power through the SMA connector to the rectifier in a wired fashion. The test result is shown in Fig. 14(a). Secondly, the rectifier was connected to a loop antenna on the PCB, and the power is transferred wirelessly from another loop antenna connected to a power amplifier with 25-dB gain. The result is shown in Fig. 14(b). Both results show the same problem. The rectifier output voltage (unregulated Vdd) saturates early below 1.5 V. In contrast, according to the simulation, it should reach 3.3 V at 10-dBm input power and saturate at 4.5 V due to the voltage limiter. We suspect that the difference may come from undesired parasitic elements that prevent the increase of output voltage, but could not figure out what they are.

TABLE I. Power Consumption Summary

	Power Consumption
LDO for LED	7.9 μW
LDO for core system	4.9 μW
Bandgap reference	20 μW
TIA	3.3 μW
Ring oscillator for sensing	2.52 μW
Ring oscillator for reference	2.22 μW
Ring oscillator for LED	5.5 μW
Modulator	27 nW
Pulse generator	180 nW
LED	100 μW
total	146.5 μW

V. CONCLUSION

Although the wireless test could not be executed due to the failure of rectifier operation, we could experimentally check that the remaining blocks operate as we have designed. This includes the amplification of the sensing current, VCO, and the frequency modulation of pulse signals afterwards. Compared to the previous studies, the size of the implantable device was dramatically reduced and the lifetime of the sensor is expected to increase by minimizing the excitation time of the fluorescent sensor. Despite of the reduction in the duration of the excitation, the frequency modulation of pulse signal was successfully demonstrated by the sample-and-hold operation of the sensed current signal.

As differential-drive rectifier usually manipulates its body biasing to elevate power conversion efficiency, each body of transistor has the isolated region with guard-ring or deep N-well. However, the guard-ring and deep N-well technics are sometimes implemented in different way according to the process, and these stamping error was not explicitly warned in simulation. We expect the operation of the entire implantable device in the next round by modifying the problem in the rectifier.

ACKNOWLEDGMENT

This work was supported by the National Research Foundation of Korea (NRF) grant NRF-2017R1C1B2009892 and NRF-2018R1A6A1A03025708. The chip fabrication and EDA tool were supported by the IC Design Education Center (IDEC), Korea.

REFERENCES

[1] Liao, Y.T.; Yao, H.; Lingley, A.; Parviz, B.; Otis, B.P. A 3-uW CMOS Glucose Sensor for Wireless Contact-Lens Tear Glucose Monitoring. IEEE J.-Solid-State Circuits 2011, 47, 335–344.
[2] Mok, J.W.; Mun, B.H.; Lee, K.J.; Kamrani, E.; Joo, C.K.; Shin, S.; Sim, J.Y.; Myung, D.; Yun, S.H.; Bao, Z.; et al. Wireless smart contact lens for diabetic diagnosis and therapy. Sci. Adv. 2020, 6, eaba3252.
[3] Koh, A.; Kang, D.; Xue, Y.; Lee, S.; Pielak, R.M.; Kim, J.; Hwang, T.; Min, S.; Banks, A.; Bastien, P.; et al. A soft, wearable microfluidic device for the capture, storage, and colorimetric sensing of sweat. Sci. Transl. Med. 2016, 8, 366ra165.
[4] Haider, M.R.; Islam, S.K.; Mostafa, S.; Zhang, M.; Oh, T. Low-power low-voltage current readout circuit for inductively powered implant system. IEEE Trans. Biomed. Circuits Syst. 2010, 4, 205–213.
[5] Mujeeb-U-Rahman, M.; Nazari, M.H.; Sencan, M.; Van Antwerp, W. A Novel Needle-Injectable Millimeter scale Wireless Electrochemical Glucose Sensing Platform for Artificial Pancreas Applications. Sci. Rep. 2019, 9, 1–11.
[6] Hassan, R.S.; Lee, J.; Kim, S. A minimally invasive implantable sensor for continuous wireless glucose monitoring based on a passive resonator. IEEE Antennas Wirel. Propag. Lett. 2019, 19, 124–128.
[7] Otis, B. Update on our Smart Lens program with Alcon. Nov 16, 2018. Available online: https://verily.com/blog/update-onour-smart-lens-program-with-alcon/ (accessed on Jan. 25, 2023.)
[8] H. Lee, J. Lee, H. Park, M. S. Nam, Y. J. Heo, and S. Kim, “Batteryless, miniaturized implantable glucose sensor using a fluorescent hydrogel,” Sensors, vol. 21, no. 24, p. 8464, 2021.
[9] Y. J. Heo, H. Shibata, T. Okitsu, T. Kawanishi, and S. Takeuchi, “Long-term in vivo glucose monitoring using fluorescent hydrogel fibers,” Proceedings of the National Academy of Sciences, vol. 108, no. 33, pp. 13 399–13 403, 2011.
[10] A. DeHennis, S. Getzlaff, D. Grice, and M. Mailand, “An nfc-enabled cmos ic for a wireless fully implantable glucose sensor,” IEEE journal of biomedical and health informatics, vol. 20, no. 1, pp. 18–28, 2015.
[11] A. S. Y. Poon, S. O'Driscoll and T. H. Meng, "Optimal Frequency for Wireless Power Transmission Into Dispersive Tissue," in IEEE Transactions on Antennas and Propagation, vol. 58, no. 5, pp. 1739-1750, May 2010.
[12] S. Kim, J. S. Ho, and A. S. Y. Poon, “Midfield Wireless Powering of Subwavelength Autonomous Devices,” Physical Review Letters, vol. 110, no. 20, May 2013.
[13] K. Kotani, A. Sasaki and T. Ito, "High-Efficiency Differential-Drive CMOS Rectifier for UHF RFIDs," in IEEE Journal of Solid-State Circuits, vol. 44, no. 11, pp. 3011-3018, Nov. 2009.
[14] Razavi, Behzad. Design of Analog Cmos Integrated Circuits. Boston, MA: McGraw-Hill, 2001.
[15] Graeme, J.G. (1996). Photodiode Amplifiers: OP AMP Solutions. Gain technology. McGraw-Hill Education. ISBN 978-0-07-024247-0. Retrieved 12 November 2020.
[16] Razavi, B. (1995). Principles of data conversion system design. New York: IEEE Press.

Hyeonkeon Lee received the M.S. degrees in electrical engineering from Kyung Hee University, Seoul, Korea, in 2021. His research interest includes RF circuits and linear RF transmitters for wireless communications. Especially, he is currently conducting the research on RF Seeker at LIG Nex1 Co.

Honghyeon Park received the M.S. degrees in electrical engineering from Kyung Hee University, Seoul, Korea, in 2022. His research interest includes analog circuits and wireless power transfer. Especially, he is currently conducting the research on PMIC at Silicon Mitus Inc.

Sanghoek Kim received the B.S. degree with a double major in Electrical Engineering and Mathematical Science from Seoul National University, Korea, in 2007, and the M.S./Ph.D. degree in Electrical Engineering from Stanford University, USA, in 2013. He was the recipient of Stanford Fellowship and Kwanjeong Scholarship during the study. After the graduation, he has worked at Qualcomm Inc. as a signal/power integrity engineer and in SiBeam, Inc as a mmWave system engineer. In 2016, he joined the EE department of Kyung Hee University, where he is now an associate professor. In 2021, he received the Young Researcher Award from the Korean Institute of Electromagnetic Engineering and Science.

Currently, his research focuses on applications of radio-frequency technology and electromagnetics theory in wireless interface with bio-implantable devices, wireless power transfer, and radar technologies.